Electroactive Interpenetrated Biohydrogels as Hybrid Materials Based on Conducting Polymers

Brenda G. Molina, Ariadna Llampayas, Georgina Fabregat, Francesc Estrany, Carlos Alemán,* and Juan Torras**

Dr. B. G. Molina, Ms. A. Llampayas, Dr. G. Fabregat, Dr. F. Estrany, Prof. C. Alemán, Dr. J. Torras

Departament d'Enginyeria Química, EEBE, Universitat Politècnica de Catalunya, C/ Eduard Maristany 10-14, 08019 Barcelona, Spain
E-mail: francesc.estrany@upc.edu; carlos.aleman@upc.edu; joan.torras@upc.edu

Dr. B. G. Molina, Dr. G. Fabregat, Dr. F. Estrany, Prof. C. Alemán, Dr. J. Torras

Barcelona Research Center for Multiscale Science and Engineering, Universitat Politècnica de Catalunya, Eduard Maristany 10-14, 08019 Barcelona, Spain

Abstract

Different levels of interpenetration of poly(hydroxymethyl-3,4-ethylenedioxythiophene) (PHMeDOT) inside a poly-γ-glutamic acid (γPGA) biohydrogel matrix, previously loaded with microparticles of poly(3,4-ethylenedioxythiophene) (PEDOT), have been obtained. The degree of interpenetration has shown influence on the morphological and electrochemical properties of the resulting biohydrogel ([PEDOT/γPGA]PHMeDOT) with a maximum after 1 hour of PHMeDOT polymerization time. The high biocompatibility of all biohydrogel components, together with the combination of mechanical properties of γPGA hydrogels with the electrochemical properties of inter-connected microparticles of PEDOT, makes it a promising material for next generation of biosensors.

1. Introduction

During the past decade, a growing number of contributions have been performed on the development of novel, nature inspired, biodegradable and biocompatible organic materials to be applied in situations where rigid conductive inorganic materials might fail.[1] These novel materials and device architectures types, when are applied to different electronic devices, could be clustered under the umbrella of the so named "green electronics".[2] Among them, organic bioelectronics is a successful emerging area of application with high potential interesting devices, such as wearable diagnostic implants and points-of-care, surgical platforms, soft robotics and disposable electronics.[2, 3] However, flexible and wearable bioelectronics demands novel electrodes design to achieve high performance in flexible electronic appliances such as wearable devices, roll-up displays, artificial skins, and implantable medical devices.[4]

Discussions regarding materials that could be used to construct flexible freestanding electrodes for energy storage or other flexible electronic devices have dominated research in recent years.[4-9] Particular attention should be paid to the electrically conductive hydrogels (ECHs) as an emerging class of hydrogels with interesting properties, which allows to easily combine the structural properties of an hydrophilic matrix with the electric conductivity of the filler material occupying the voids of the hydrogel matrix. The most usual filler materials are metallic nanoparticles, conducting polymers (CPs), graphene, composites, silicon-based, or transition metal oxide-based materials.[10] The good electrical conductivity and the self-healing, adhesivity, flexibility and biocompatibility properties of some ECHs [11, 12] allow us to glimpse these new materials with a very promising future for their application in tissue regeneration, drug release and wearable sensors, among others. [13-16]

Currently, poly(3,4-ethylenedioxythiophene) (PEDOT) is one of the most employed CPs, which can be easily obtained by anodic polymerization in different conditions and holding a high biocompatibility.[17-19] Similarly, poly(hydroxymethyl-3,4-ethylenedioxythiophene)

(PHMeDOT) has shown a higher conductivity, better electrochemical properties, and a better biocompatibility than PEDOT. [20] On the other hand, poly-γ-glutamic acid (γPGA) is a naturally synthesized polymer by some microbial strains such as the *Bacillus subtilis*, among others.[21, 22] More specifically, It is an anionic homopolypeptide exhibiting good biocompatibility, biodegradability, water-solubility and no human toxicity.[23] The γ-PGA can be cross-linked to produce biohydrogels with interesting additional biophysical properties, but still maintaining its biocompatibility.[24-26] The combination of these elements to build a flexible electrode will open the opportunity not only to biocompatible and wearable energy storages but also to the green electronics building novel implantable devices. Recently, we developed conductive polymer-based hydrogels using either cellulose[27] or γPGA[28, 29] as a biohydrogel matrix to be used in both flexible electrodes and energy storage applications. These latter works have established a new methodology, in which two different types of conductive fillers are synergistically combined and, thus, improving the conductivity properties of the material as a whole. More specifically, the hydrogel matrix was loaded with conducting polymer microparticles (CPMs) of PEDOT during the cross-linking step, the resulting material being denoted. After this, the CPMs were inter-connected among them through an anodic polymerization with a similar conducting polymer in aqueous medium to create inter-penetrated network with multiple and stable conduction paths. The resulting hybrid disclosed excellent stability after 2000 charge-discharge cycles with a specific capacitance loss of only 8%.[29] This methodology can be easily extended to other CPs and hydrogel matrixes.

As previous research was focused on the fabrication of an integrated energy storage device, a deep investigation on the formation mechanism of the interpenetrated conduction paths is expected to help to energy storage capacity by controlling the polymerization time and the hybrid material components. Up to our knowledge, this is the first time that the formation of the micro-connection paths within an electroactive material will be studied and verified by

means of relating between the structure and conductivity of its constituents. The aim of this work is focused on the study of an interpenetrating polymer network (IPN) hydrogel made of γPGA biohydrogels and CP microparticles, which have been inter-connected by means of *in-situ* electropolymeritzation of poly(hydroxymethyl-3,4-ethylenedioxythiophene) (PHMeDOT). The biocompatibility of PEDOT and PHMeDOT CPs has been verified elsewhere through in vitro and in vivo studies.[30] The electro-physical and structural properties of this material, hereafter denoted [PEDOT/γPGA]PHMeDOT, have been evaluated as a function of the time used for the PHMeDOT polymerization. Finally the novel hydrogel material was used to test its biosensor capabilities by detecting the levofloxacin antibiotic. Results evidence the formation of conduction path connecting different CPMs through all the internal IPN-structure.

2. Results and Discussion

2.1. Preparation of [PEDOT/γPGA]PHMeDOT material

The inclusion of PEDOT microparticles (MPs) within supporting materials with poor, or even null, electric properties such as the γPGA and cellulose, but holding interesting properties (i.e., non-toxicity and biocompatibility) to be considered part of novel electroactive biomaterials for energy storage applications, has been previously reported by the authors.[27, 28] In this work, the synthesis of PEDOT/γPGA and [PEDOT/γPGA]PHMeDOT materials was conducted following a methodology similar to that reported by Saborio et al.[28] In brief, this process can be summarized in four steps: i) Preparation of PEDOT films by CA using a 10 mM monomer solution in acetonitrile with 0.1 M $LiClO_4$ as reaction medium (**Figure 1a**); ii) Processing of PEDOT films into MPs by mechanical dispersion in a 0.5 M $NaHCO_3$ aqueous solution (Figure 1b); iii) Synthesis of a self-standing PEDOT/γPGA hydrogel dissolving γPGA polymer in a 0.5 M $NaHCO_3$ solution containing the PEDOT MPs and using cystamine and 1-[3-(Dimethylamino)propyl]-3-ethyl carbodiimide (EDC) as cross-linker and activating agent, respectively (Figure 1c); and iv) *in situ* electrochemical polymerization of PHMeDOT inside

the PEDOT/γPGA hydrogel (Figure 1d), which was achieved by submerging overnight the PEDOT/γPGA hydrogel into an aqueous solution of 10 mM HMeDOT monomer and 0.1M $LiClO_4$ (i.e. this process ensured the penetration of the monomer into the hydrogel matrix). More details on the [PEDOT/γPGA]PHMeDOT biohydrogel synthesis can be found on the methods section within the supplementary information.

The successful incorporation of PEDOT MPs inside the γPGA hydrogel was corroborated by energy dispersive X-ray (EDX) spectroscopy and micro-Raman spectroscopy. **Figure 2** shows a representative SEM micrograph of the PEDOT/γPGA hydrogel and the results from EDX analyses on two different surface points (i.e. at the PEDOT MPs and at the γ-PGA hydrogel matrix). As is shown, EDX enables the detection of S and Cl elements among others at specific points on the surface. Although the S signal can be attributed to both the Cys crosslinker and the thiophene ring of PEDOT, the Cl element is ascribed only to the ClO_4^- dopant of PEDOT MPs, allowing an easy differentiation between the MPs and the γ-PGA hydrogel matrix. Furthermore, Raman spectra were taken from PEDOT/γPGA samples using confocal Raman microscope. Spectra were taken inside an area of the sample, were black spots ascribable to the PEDOT particles was clearly identified. The spectra reported in **Figure 2d** exhibit the characteristics peaks of PEDOT: 983 cm^{-1} (vibration mode of the thiophene C–S bond), 1085 cm^{-1} (stretching of the ethylendioxy group), 1255 cm^{-1} (C–C inter-ring stretching), 1365 cm^{-1} (C–C stretching), 1430 cm^{-1} (C=C symmetrical stretching) and 1485 cm^{-1} (C=C asymmetrical stretching). Additionally, **Figure S1** shows the micro-Raman spectra on the IPN-hydrogel of PEDOT/γPGA sample. It is observed the characteristics peak of γPGA: 950 cm^{-1} (C–C stretching), 1030 cm^{-1} (COC stretching), 1440 cm^{-1} (CH_2 scissoring), 1658 cm^{-1} (C=O stretching) and 2926 cm^{-1} (CH_2 asymmetrical stretching). Therefore, we conclude that PEDOT MPs are well and homogenously distributed inside the IPN-hydrogel of PEDOT/γPGA.

The FTIR spectra of PEDOT and γPGA are shown in Figure 3a and b, respectively. Also, Table S1 lists main FTIR peaks. PEDOT exhibits characteristic adsorption bands at 1474 and 1512 cm^{-1} (symmetric C=C stretching), 1200 cm^{-1} (assymmetric C–O–C stretching), 1019 cm^{-1} (symmetric C–O–C stretching), and 965 and 911 cm^{-1} (C–S stretching).[31] Besides, the typical bands of absorption of the γPGA matrix, which were previously identified by Pérez-Madrigal et al.,[32] appear at 3275 cm^{-1} (N–H stretching from the amide), 2927 cm^{-1} (symmetric CH_2 stretching), 1621 cm^{-1} (C=O stretching), 1535 cm^{-1} (NH amide II) and 1400 cm^{-1} (CH_2 wagging).

On the other hand, percolation of PEDOT MPs has been achieved by forming of conduction paths made of PHMeDOT doped with ClO_4^- that inter-connect such MPs, which in turn act as polymerization nuclei during the electrogeneration of the latter CP.[28] The formation of such conduction paths have been investigated by considering different polymerization times (θ) for PHMeDOT. Figure 3c compares the FTIR spectra [PEDOT/γPGA]PHMeDOT systems prepared using θ = 15 min, 30 min, 1 h, 4 h, 7 h and 10 h. In all cases, the absorption bands associated to both PEDOT MPs and γPGA are observed. It is worth to notice that the bands of the PHMeDOT hydroxyl group and the γPGA hydrogel amide group overlap at about 3270 cm^{-1}, unambiguous identification being impossible. The existence of secondary amides in the chemical composition of the hydrogels is observed by the C=O bond stretching (1621 cm^{-1}) and the N–H of amide II (1535 cm^{-1}). Besides, the presence of the ethylenedioxy moiety is detected at 1030 cm^{-1} (symmetric COC stretching) and 1187 cm^{-1} (asymmetric COC stretching), while the C=C stretching appears at 1455 cm^{-1}. The variation of the bands located between 1530 and 1700 cm^{-1} with θ was previously attributed to an over-oxidation process of the γPGA hydrogel matrix.[28]

Table 1 lists and **Figure S2** shows the averaged swelling ratio (SR) values obtained for all prepared hydrogels. All of them have a very high SR in water, increasing its weight up to 8000%, which corresponds to the bare γPGA hydrogel without CP loaded. Differences

between them are mainly due to the chemical composition. The γPGA hydrogel presents the highest swelling ratio among all hydrogels generated in this work (SR = 8052% ± 1176%). The reason lies on the absence of PEDOT MPs inside since identical γPGA/EDC/cystamine molar ratios were used for the synthesis of γPGA, PEDOT/γPGA and [PEDOT/γPGA]PHMeDOT hydrogels. Representative SEM micrographs of γPGA hydrogels reflect a high density of pores with average diameter 6.9 ± 1.8 μm (**Figure 4a** and 4b). Interestingly, the incorporation of PEDOT MPs inside the γPGA matrix decreases the water absorption capacity to 6324% ± 910%. Although PEDOT is a hydrophilic CP, its affinity towards water is significantly lower than that of γPGA, limiting the ability of PEDOT/γPGA to absorb water.

On the other hand, analysis of the swelling behavior of [PEDOT/γPGA]PHMeDOT hydrogels indicates that the incorporation of PHMeDOT slightly improves the water absorption capacity with respect to PEDOT/γPGA. The SR increases with the electrogeneration time until a maximum is reached at θ = 1 h (SR = 6805% ± 1018%). It is worth noting that HMeDOT monomer presents higher water solubility when it is compared with EDOT monomer. Thus, it is expected that PHMeDOT is slightly more hydrophilic than PEDOT due to the exocyclic hydroxymethyl group, which explains the slight increment in the SR values. However, the SR of hydrogels prepared using θ > 1 h decreases with increasing polymerization time. This phenomenon can be caused by both the micropore clogging effect and degradation underwent by the γPGA matrix, which will be discussed below.

SEM micrographs of freeze-dried hybrid hydrogels using two different magnifications are shown in Figure 4c-h, which correspond to the front side of the hydrogel (i.e. polymer side in contact with the working electrode). IPN-structure, which give rise to dense and open macroporous hydrogel networks, are observed in all cases. Inclusion of PEDOT MPs (Figure 4c and d) leads to a pores with average size of 20.8 ± 5.4 μm distributed throughout the

PEDOT/γPGA hydrogel, which are significantly larger than pores displayed in Figure 4a and b for γPGA. In addition, PEDOT MPs with a size between 5 and 15 μm can be distinguished scattered throughout the surface and inside the hydrogel. The existence of PEDOT MPs is confirmed with the help of the EDX density map (**Figure S3**). The higher density associated to the sulphur atoms, which is enhanced by a green scale color in the two-dimensional EDX surface, indicates the location of PEDOT MPs.

Especially interesting is the morphology that presents [PEDOT/γPGA]PHMeDOT (θ = 1 h, Figure 4e and f) hydrogel with a very porous surface but with micropores a little bit smaller (12.3 ± 4.9 μm of average diameter) than PEDOT/γPGA. In fact, the observed surface presents a different morphology with a very open structure, which might explain its high observed capacity to absorb water (SR = 6805 ± 1018 %, the highest among all hydrogels with electrogenerated PHMeDOT). These IPN-matrix properties favor the rapid transport of ions and electrons during redox electrochemical processes and, therefore, higher levels of charge storage and pseudocapacitance are expected for this material. Instead, the porosity decreases for [PEDOT/γPGA]PHMeDOT (θ = 4 h) hydrogel (Figure 4g-h). Moreover, EDX density maps for oxygen and sulphur atoms (Figure S3b) reveals that PHMeDOT clusters are interconnected among them and are also connected to different PEDOT MPs. Figure 4g-h shows that the surface is rougher not so porous and much more closed. However, the pores present have a much larger size (112.4 ± 82 μm) than those of [PEDOT/γPGA]PHMeDOT (θ = 1 h) (12.3 ± 4.9 μm), presenting a disorderly and non-homogeneous distribution which might also indicates some degradation on the γPGA matrix (**Figure S4**). This closed structure of [PEDOT/γPGA]PHMeDOT (θ = 4 h) is consistent with its the SR value (Table 1), which is one of the lowest among all prepared hydrogels.

2.2. Electrochemical Characterization

The electrical response of PEDOT films, before being transformed into MPs, was characterized by cyclic voltammetry (CV). The electrolytic cell contained an aqueous solution

of 0.1 M $LiClO_4$ as supporting electrolyte, voltammograms being recorded in the potential interval from −0.50 V to 1.10 V at a scan rate of 100 mV s^{-1}. The reversal potential, 1.1 V, was set to the same value used for the electrochemical characterization of γPGA, PEDOT/γPGA and [PEDOT/γPGA]PHMeDOT hydrogels in aqueous medium (see below), which was restricted by the standard reduction potential of water. Comparison of the voltammograms recorded for PEDOT during 30 consecutive oxidation-reducing cycles reflected a very high electrochemical stability (not shown). In fact, the anodic and cathodic areas remained practically unaffected, indicating an almost constant electroactivity system, with a reduction of only 2% after 30 cycles. These results are in agreement with the previously reported electrochemical behavior of PEDOT.[33]

The characterization of hydrogels supported on ITO electrodes was conducted using the same methodology. Table 2 lists the loss of electroactivity (LEA) between the 2nd and 30th cycle and the specific capacitance (SC) values for the studied hydrogel materials. It is clearly observed an enhancement of the electrochemical activity when PEDOT MPs are incorporated inside the γ-PGA hydrogel, which behaves as a dielectric material.[28, 29, 32] Indeed, the SC is greater for the hybrid PEDOT/γPGA system than for the bare γPGA hydrogel by one order of magnitude. However, comparing the loss of electrostability it is high and similar for both systems (i.e. ~ 40%).

It is known that, in general, the electroactivity of the PEDOT/γPGA hydrogel increases drastically with the *in-situ* electropolymerization of the PHMeDOT polymer in its matrix.[27, 28, 34] Indeed, it is postulated that PEDOT MPs ensure dispersion of the PHMeDOT throughout the hydrogel since they act as nucleation points, stimulating the interpenetration of the grown CP chains.[28] In addition, the PHMeDOT hydrophilicity plays an important role in its electropolimerization in aqueous media. More specifically, the higher solubility of the HMeDOT when compared to EDOT monomer facilitates its preparation within the hydrated γ-PGA matrix.[34] However, both the optimal polymerization time for PHMeDOT inside the

PEDOT/γPGA hydrogel and the relationship between morphology and the electrochemical properties of [PEDOT/γPGA]PHMeDOT hydrogel remain unkown. In order to provide some understanding on these points, the IPN-hydrogels obtained using different electropolymerization times for PHMeDOT were evaluated by CV. **Figure S5** presents, one by one, the 6 series of voltammograms obtained for each IPN-hydrogel (θ = 15 min, 30 min, 1 h, 4 h, 7 h and 10 h), showing both redox cycle 2 and 30 for each one.

In all cases, a decrease in the electroactivity with successive redox cycles is observed. The area reduction as the number of cycles increases is relatively small compared with the area of the first cycle, which indicates that all IPN-hydrogels have a good electroestability. In addition to this general effect, detailed inspection on the different voltammetric curves allows us a more accurate analysis and a better discrimination among them. **Figure 5** presents in a single graphic the voltammogram recorded for the second redox cycle of all studied systems. It is important to notice that the [PEDOT/γPGA]PHMeDOT hydrogel obtained using θ = 1 h shows an anodic intensity value much higher than the other systems, thus reflecting much better electroactivity in this material. Moreover, the [PEDOT/γPGA]PHMeDOT (θ =1 h) hydrogel has a redox storage capacity much higher than others system, in either smaller or larger θ values.

On the other hand, additional information can be obtained by examining the shape of the voltammograms shown in **Figure S5**. The [PEDOT/γPGA]PHMeDOT (θ = 15 min) hydrogel presents a symmetrical curve, whereas the one prepared using θ = 30 min exhibits a change in the slope at ~0.25 V, with some asymmetry. Interestingly, [PEDOT/γPGA]PHMeDOT (θ = 1 h) displays an almost ideal symmetrical shape, being by far the one with the highest electroactivity. Moreover, the voltammograms of the IPN-hydrogels obtained using θ = 4, 7 and 10 h show asymmetrical profiles, with changes in the slope and even concavity change points in the anodic and/or cathodic scans. Such three IPN-hydrogels exhibit a redox capacity that is ten times lower than the one prepared using θ =1 h.

Based on these observations, it is concluded that the most symmetrical CV curve is obtained for the IPN-hydrogel with greatest electroactivity (i.e. [PEDOT/γPGA]PHMeDOT (θ = 1 h)). The asymmetric voltammograms with a variation in the current-density slope present much lower redox capacity of charge storage. The voltammogram obtained for [PEDOT/γPGA]PHMeDOT (θ = 1 h) indicates that such hydrogel exhibits a surface much more open than the others interpenetrated systems, providing a very good ionic mobility through the hydrogel/electrolyte interface. In addition, it is observed a great structural homogeneity, not presenting preferential zones of oxidation at a given potential that would bring about changes in the slope of the anodic current. Instead, IPN-hydrogels prepared using θ = 30 min and, especially, θ > 1h show asymmetrical CV curves that are consistent with a non-homogeneous structure and preferential oxidation zones with the corresponding reduction regions.

Considering the results obtained and the above observations, the following reasoning can be stated. The formation of the PHMeDOT connections between PEDOT MPs has an initial effect (first 15 minutes) of opening and enlargement of the pores of the hydrogel surface, then passing through a stage in which there is also contribution of folding effects of the hydrogel matrix. At this point the specific interfacial surface is reduced (with a certain decrease in electroactivity at θ = 30 min). Longer operating times applying the external electric field, the yielding process of PHMeDOT-connections continues, which is affecting a greater percentage of the hydrogel matrix, within the aggregates and folds that have been formed. This phenomenon leads to an increasingly homogeneous morphology where the specific interfacial surface increases up to fill all the polymer matrix points where the formation of the PHMeDOT-connections is possible, which happens about at θ = 1 h.

Figure S6 shows the SC values of the hybrid hydrogels obtained at the different θ values as a function of the number of oxidation-reduction cycles. It is observed how the SC values are kept close to the initial value, indicating that the material structure is well defined and has

good electrostability, independently of θ. It is noteworthy the case of [PEDOT/γPGA]PHMeDOT (θ = 1 h) hydrogel, which undergoes a small increase of its SC after several consecutive oxidation-reduction cycles. More specifically, its SC values goes from 4.4 mF cm^{-2} up to 4.6 mF cm^{-2} after 30 redox cycles (see Table 2). This fact suggests a small structural rearrangement,[28] probably due to the retention of small residual amounts of monomer within the hydrogel matrix that are polymerized in the successive anodic scanning. Therefore, a slight increase in its specific interfacial surface is expected. Quantification of the electrochemical effect of the PHMeDOT incorporation in PEDOT/γPGA hydrogel is provided in Table 2. More specifically, the SC is approximately 50 times higher of [γ-PGA/PEDOT] PHMeDOT (θ = 1 h) than PEDOT/γPGA (see Table 2) and very similar to that reported by the well-known organic electrodes of PEDOT:PSS (4.7 mF cm^{-2})[35] but with additional flexibility and biocompatibility properties due to the hydrogel matrix.

The maximum electroactivity obtained for the [PEDOT/γPGA]PHMeDOT (θ = 1 h) coincides with the highest SR. Also, at longer electrogeneration times, both electrochemical properties and SR present similar behavior with a significant decrease of those properties. This has been attributed to an over-oxidation of ECP components (confirmed by the FTIR spectra) and the degradation of some component of the hydrogel itself (mainly the γPGA), which would be related to the above-mentioned folds in SEM micrographs (Figure 4) that obstruct the pores.

2.3. Hydrogel as a potential biosensor

Previous studies have been proved that conductive polymers, through electrochemical assays, i.e., cyclic voltammetry and square wave voltammetry, can be used as sensitive and selective sensors for the determination of the levofloxacin (LEV), an antibiotic of fluoroquinolones (FQs) family, even in biological samples.[36-38] Moreover, hydrogels with good electrochemical properties, such as tunable conductivity and reversible oxidation/reduction processes, have been shown as an excellent carrier matrixes and efficient electrodes, suitable

to be used in a dual-function integrated system. For instance, on the monitoring in real time the release of previously loaded molecules in the hydrogel matrix.[39, 40]

As proof of concept in the use of this new material as a potential biosensor, a [PEDOT/γPGA] PHMeDOT electrode was used for LEV determination. **Figure S7** displays the second cyclic voltammogram of a PHMeDOT film, electrodeposited by CA during 600 seconds, in a 0.1M $LiClO_4$ solution with and without 0.2 mM of LEV. The oxidation peak potential of LEV at the polymer film is clearly identified at 1.17 V. Similar results were obtained when the same amount of antibiotic was load into the system [PEDOT/γPGA] PHMeDOT (θ = 1 h), by absorption, as can be observed in **Figure 6**. These results show this promising new material within a future area of interest for the use of electroactive hydrogels as integrated dual-function systems.

3. Conclusion

In summary, we have studied the influence of different levels of interpenetration of PHMeDOT inside the PEDOT/γPGA hydrogel, and their influence on the morphological and electrochemical properties of the resulting material with a high potential to be used as a flexible electrode in biocompatible devices. A polymerization time of θ = 1 h has been demonstrated as the optimum to obtain the best electrochemical properties of the material with a high specific capacitance. Also, the improvement of electrochemical properties is being accompanied by a maximum swelling ratio. The [PEDOT/γPGA]PHMeDOT (θ = 1 h) hydrogel exhibits an open internal structure that facilitates diffusion processes as well as the inter-connection among PEDOT MPs by conduction paths. At higher polymerization times, a decreasing on the electrochemical response was observed. This occurs mainly for two reasons: an over-oxidation of the conducting polymers and the γPGA hydrogel matrix degradation itself. Finally, the novel electroactive hydrogel material has been shown as a potential biosensor, thus being able to detect the levofloxacin antibiotic. Combining the

biocompatibility and mechanical properties of γPGA hydrogels with the electrochemical properties of inter-connected microparticles of biocompatible PEDOT by means of conducting paths, makes it a promising material for next generation of biosensors.

4. Experimental Section

Materials: Cystamine dihydrochloride (Cystamine; >=98%), 1-[3-(Dimethylamino)propyl]-3-ethyl carbodiimide (EDC), 3,4-ethylenedioxythiophene (EDOT, 97%), and hydroxymethyl (3,4-ethylenedioxythiophene) (HMeDOT, 95 %) were purchased from Sigma-Aldrich. Poly-γ-glutamic acid (γPGA) of low molecular weight (M_w = 200,000-500,000) was purchased from Wako Chemicals GmbH. EDOT and HMeDOT monomers were used as received. Lithium perchlorate ($LiClO_4$) was obtained from Sigma-Adrich, and it was stored in an oven at 70 ºC before use as a dopant agent in the electrochemical generation of polymer. Acetonitrile (ACN) solvent was purchased from Panreac. Milli-Q water grade (0.055 μS cm^{-1}) was used in all the synthesis processes.

PEDOT microparticles: PEDOT films were prepared by chronoamperometry (CA) at +1.40 V in an acetonitrile solution containing EDOT (10mM) and $LiClO_4$ (0.1M) as supporting electrolyte. The use of ACN instead of water will allow us to apply the optimal constant potential of 1.40 V, which is larger than the water splitting potential. The experimental set-up for this anodic polymerization was described in previous work.[33] PEDOT was processed into particles using a vortex at maximum power during two hours and dispersed (20% w/w) in basic aqueous solution (0.5 M $NaHCO_3$) through magnetic agitation (500 rpm) during one week. The resulting PEDOT particles were employed for the synthesis of loaded γPGA hydrogels.

Preparation of PEDOT/γPGA material: The γPGA hydrogels loaded with PEDOT particles, hereafter denoted PEDOT/γPGA, were prepared adapting the procedure described by Matsusaki *et al.*[41] Specifically, γPGA (0.5 unit mmol) and EDC (0.4 mmol) were dissolved

in a solution of $NaHCO_3$ (0.75 mL of 0.5 M) containing PEDOT particles (20% w/w) at 4 °C under magnetic stirring. Then, cystamine dihydrochloride (0.2 mmol), previously dissolved in a sodium hydrogen carbonate solution (0.25 mL of 0.5 M), was added to the solution and mixed during 2−3 min. The γ-PGA/EDC/cystamine molar ratio between the three compounds was set to 5/4/2 (expressed in units of mol). The final solution was removed with a magnetic stirrer, and the reaction solution was poured into glass molds of 5.0 × 2.5 × 0.1 cm^3 with one face made of indium-tin oxide/polyethylene terephthalate (ITO/PET) electrode. The solution was let to gel at 4 °C for 1 h. To remove any compound in excess, the resulting hydrogel was washed with phosphate-buffered saline (PBS) solution three times during 20 minutes each.

Preparation of [PEDOT/γPGA]PHMeDOT material: ITO/PET electrodes of 5.0 × 4.0 cm^2 were coated with PEDOT/γPGA hydrogel and subsequently kept in the reaction medium overnight at 4° C. The PEDOT/γPGA coated sheets were then used as working electrodes for the anodic polymerization of PHMeDOT by CA. The reaction medium was an aqueous solution of HMeDOT (10 mM) with $LiClO_4$ (0.1 M) as the supporting electrolyte. A set of anodic polymerizations were conducted under a constant potential of +1.10 V using different polymerization times (i.e., θ = 15 min, 30 min, 1 h, 4 h, 7 h, and 10 h). The experimental setup used for the in situ modification of the PEDOT/γ-PGA hydrogel and electrochemical assays were performed with a potentiostat-galvanostat Autolab PGSTAT101 equipped with the ECD module (to facilitate low currents measurement) using a three-electrode compartment cell at room temperature. The working and counter electrodes were cleaned with acetone, ethanol and distilled water before each trial to prevent interferences along electrochemical assays. The reference electrode was an Ag|AgCl electrode containing a KCl saturated aqueous solution (offset potential versus the standard hydrogen electrode, E^o = 0.222 V at 25ºC). Hereafter, the loaded PEDOT/γPGA hydrogel electrochemically modified with in situ polymerization of HMeDOT is denoted [PEDOT/γPGA]PHMeDOT.

Morphological, chemical and electrochemical characterization: Detailed inspection of the samples was conducted by scanning electron microscopy. A compact Phenom XL Desktop SEM, acquired from PhenomWorld, equipped with an EDS (micro-analysis) detectors and operating at 15 kV was used. The different freeze-dried samples were supported onto a double-sided adhesive carbon disc and were sputter-coated with a thin layer of carbon to prevent sample charging problems using a K950X Turbo Evaporator. The diameter of the perforations was measured with Image J software.

FTIR spectra of PEDOT film and freeze-dried γPGA, PEDOT/γPGA, and [PEDOT/γPGA] PHMeDOT hydrogels were recorded on a FTIR Jasco 4100 spectrophotometer. Samples were placed by an attenuated total reflection accessory with a diamond crystal (Specac model MKII Golden Gate Heated Single Reflection Diamond ATR). A total of 64 scans were performed between 4000 and 600 cm^{-1} for each sample with a resolution of 4 cm^{-1}.

Micro-Raman spectroscopy was used to characterize some samples using a commercial Renishaw inVia Qontor confocal Raman microscope. The Raman spectra was made by a laser beam (785 nm with a nominal 300 mW output power), which was directed through a microscope (specially adapted Leica DM2700 M microscope) to the sample. The scattered light was collected and directed to a spectrometer with a 1200 lines·mm^{-1} grating. A time exposition of 1s was used and the laser power was adjusted to 1% of its nominal power.

The swelling ratio (SR, in %) of the resulting modified γPGA hydrogels was determined according to:

$$SR(\%) = \frac{w_W - w_D}{w_D} x100 \qquad (1)$$

where w_W is the weight of the hydrogels after 24 hours plunged in distilled water and w_D is the weight of the hydrogel after freeze-drying (dried hydrogel).

Cyclic voltammetry (CV) was carried out to evaluate the electroactivity, areal specific capacitance (SC), and the electrochemical stability of hybrid material. The initial and final

potentials were −0.50 V, and the reversal potential was +1.10 V. A scan rate of 100 mV s^{-1} was used in all cases. All electrochemical experiments were run in triplicate using water with $LiClO_4$ (0.1 M) as supporting electrolyte.

The areal SC (in mF cm^{-2}) was determined using the following expression:

$$SC = \frac{Q}{\Delta V \cdot A} \quad (2)$$

where Q is the charge determined by integrating either the oxidative or the reductive parts of the cyclic voltammogram curve, ΔV is the potential window (in V), and A is the electrode area (in cm^2). The exposed area of the different electrodes for CV analyses was 0.5 cm^2. The measurement of the loss of electroactivity (LEA, in %) against the number of oxidation−reduction cycles will allow to determine the electrochemical stability of the sample:

$$LEA = \frac{\Delta Q}{Q_2} = \frac{Q_i - Q_2}{Q_2}\, x100 \quad (3)$$

where ΔQ is the difference between the oxidation charge (in C) of the second (Q_2) and the evaluated oxidation−reduction cycle (Q_i). The first cycle at the experimental level is really discarded, since a structural relaxation of the polymer that forms the film is always necessary, which takes place in the 1st redox process. Thus, it is the second cycle, which is considered as reference to obtain the loss of electroactivity.

Supporting Information

Supporting Information is available from the Wiley Online Library or from the author.

Acknowledgements

Authors acknowledge MINECO/FEDER (RTI2018-098951-B-I00) and the Agència de Gestió d'Ajuts Universitaris i de Recerca (2017SGR359) for financial support. B. G. M. is thankful to CONACYT agency for their financial support through a postgraduate scholarship (328467

CVU 621314). Support for the research of C.A. was received through the prize “ICREA Academia” for excellence in research funded by the Generalitat de Catalunya

Received: ((will be filled in by the editorial staff))
Revised: ((will be filled in by the editorial staff))
Published online: ((will be filled in by the editorial staff))

References

[1] C. Yang, W. Lin, Z. Li, R. Zhang, H. Wen, B. Gao, G. Chen, P. Gao, M. M. F. Yuen, C. P. Wong, *Adv. Funct. Mater.* **2011**, *21*, 4582.

[2] M. Irimia-Vladu, *Chem. Soc. Rev.* **2014**, *43*, 588.

[3] D. T. Simon, E. O. Gabrielsson, K. Tybrandt, M. Berggren, *Chem. Rev.* **2016**, *116*, 13009.

[4] Q. Li, Z. Hu, Z. Liu, Y. Zhao, M. Li, J. Meng, X. Tian, X. Xu, L. Mai, *Chemistry – A European Journal* **2018**, *24*, 18307.

[5] Q. Zheng, Z. Li, J. Yang, J.-K. Kim, *Progress in Materials Science* **2014**, *64*, 200.

[6] L. Li, Z. Wu, S. Yuan, X.-B. Zhang, *Energy & Environmental Science* **2014**, *7*, 2101.

[7] H. Lee, I. Kim, M. Kim, H. Lee, *Nanoscale* **2016**, *8*, 1789.

[8] M. Cheng, Y.-N. Meng, Z.-X. Wei, *Isr. J. Chem.* **2018**, *58*, 1299.

[9] J. Xing, P. Tao, Z. Wu, C. Xing, X. Liao, S. Nie, *Carbohydr. Polym.* **2019**, *207*, 447.

[10] W. Zhang, P. Feng, J. Chen, Z. Sun, B. Zhao, *Prog. Polym. Sci.* **2019**, *88*, 220.

[11] Z. Deng, T. Hu, Q. Lei, J. He, P. X. Ma, B. Guo, *ACS Applied Materials & Interfaces* **2019**, *11*, 6796.

[12] Z. Deng, H. Wang, P. X. Ma, B. Guo, *Nanoscale* **2020**, *12*, 1224.

[13] B. Guo, P. X. Ma, *Biomacromolecules* **2018**, *19*, 1764.

[14] Y. Liang, X. Zhao, T. Hu, Y. Han, B. Guo, *J. Colloid Interface Sci.* **2019**, *556*, 514.

[15] Y. Liang, X. Zhao, T. Hu, B. Chen, Z. Yin, P. X. Ma, B. Guo, *Small* **2019**, *15*, 1900046.

[16] R. Dong, P. X. Ma, B. Guo, *Biomaterials* **2020**, *229*, 119584.

[17] K. Feron, R. Lim, C. Sherwood, A. Keynes, A. Brichta, P. C. Dastoor, *International Journal of Molecular Sciences* **2018**, *19*, 2382.

[18] Y. Hui, C. Bian, S. Xia, J. Tong, J. Wang, *Anal. Chim. Acta* **2018**, *1022*, 1.

[19] L. J. del Valle, D. Aradilla, R. Oliver, F. Sepulcre, A. Gamez, E. Armelin, C. Alemán, F. Estrany, *Eur. Polym. J.* **2007**, *43*, 2342.

[20] Y. Yao, L. Zhang, Y. Wen, Z. Wang, H. Zhang, D. Hu, J. Xu, X. Duan, *Ionics* **2015**, *21*, 2927.

[21] C. B. Thorne, C. G. Gómez, H. E. Noyes, R. D. Housewright, *J. Bacteriol.* **1954**, *68*, 307.

[22] R. Chettri, M. O. Bhutia, J. P. Tamang, *Frontiers in Microbiology* **2016**, *7*.

[23] I.-L. Shih, P.-J. Wu, C.-J. Shieh, *Process Biochemistry* **2005**, *40*, 2827.

[24] M. Matsusaki, T. Serizawa, A. Kishida, M. Akashi, *Journal of Biomedical Materials Research Part A* **2005**, *73A*, 485.

[25] S. Murakami, N. Aoki, *Biomacromolecules* **2006**, *7*, 2122.

[26] M. Taniguchi, K. Kato, A. Shimauchi, P. Xu, K.-I. Fujita, T. Tanaka, Y. Tarui, E. Hirasawa, *J. Biosci. Bioeng.* **2005**, *99*, 130.

[27] M. G. Saborío, P. Svelic, J. Casanovas, G. Ruano, M. M. Pérez-Madrigal, L. Franco, J. Torras, F. Estrany, C. Alemán, *Eur. Polym. J.* **2019**, *118*, 347.

[28] M. C. G. Saborío, S. Lanzalaco, G. Fabregat, J. Puiggalí, F. Estrany, C. Alemán, *J. Phys. Chem. C* **2018**, *122*, 1078.

[29] M. G. Saborío, Š. Zukić, S. Lanzalaco, J. Casanovas, J. Puiggalí, F. Estrany, C. Alemán, *Materials Today Communications* **2018**, *16*, 60.

[30] S.-C. Luo, E. Mohamed Ali, N. C. Tansil, H.-h. Yu, S. Gao, E. A. B. Kantchev, J. Y. Ying, *Langmuir* **2008**, *24*, 8071.

[31] F. Tran-Van, S. Garreau, G. Louarn, G. Froyer, C. Chevrot, *J. Mater. Chem.* **2001**, *11*, 1378.

[32] M. M. Pérez-Madrigal, M. G. Edo, A. Díaz, J. Puiggalí, C. Alemán, *J. Phys. Chem. C* **2017**, *121*, 3182.

[33] C. Ocampo, R. Oliver, E. Armelin, C. Alemán, F. Estrany, *J. Polym. Res.* **2006**, *13*, 193.

[34] G. Fabregat, J. Casanovas, E. Redondo, E. Armelin, C. Alemán, *Phys. Chem. Chem. Phys.* **2014**, *16*, 7850.

[35] T. Cheng, Y.-Z. Zhang, J.-D. Zhang, W.-Y. Lai, W. Huang, *Journal of Materials Chemistry A* **2016**, *4*, 10493.

[36] E. Mazzotta, C. Malitesta, M. Díaz-Álvarez, A. Martin-Esteban, *Thin Solid Films* **2012**, *520*, 1938.

[37] F. Wang, L. Zhu, J. Zhang, *Sensors and Actuators B: Chemical* **2014**, *192*, 642.

[38] M. Rkik, M. B. Brahim, Y. Samet, *J. Electroanal. Chem.* **2017**, *794*, 175.

[39] G. Fabregat, A. Giménez, A. Díaz, J. Puiggalí, C. Alemán, *Macromol. Biosci.* **2018**, *18*, 1800014.

[40] B. G. Molina, E. Domínguez, E. Armelin, C. Alemán, *Gels* **2018**, *4*, 86.

[41] M. Matsusaki, H. Yoshida, M. Akashi, *Biomaterials* **2007**, *28*, 2729.

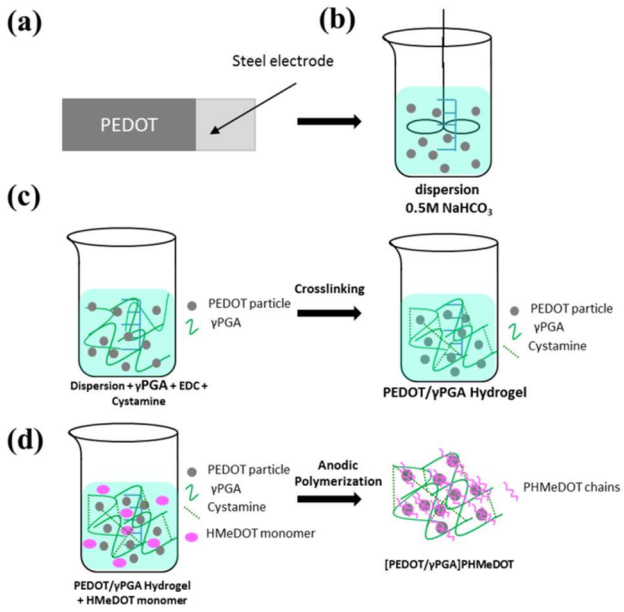

Figure 1. Scheme showing the synthetic steps used to produce [PEDOT/γPGA] PHMeDOT electrodes: (a) preparation of PEDOT films by CA; and (b) posterior dispersion by mechanical stirring to obtain CPMs; (c) formation of PEDOT/γPGA hydrogel using a γPGA/EDC/cystamine molar ratio of 5/4/2 for the crosslinking; and (d) *in situ* anodic polymerization of HMeDOT monomer using PEDOT microparticles which plays the role of polymerization nuclei to produce [PEDOT/γPGA]PHMeDOT.

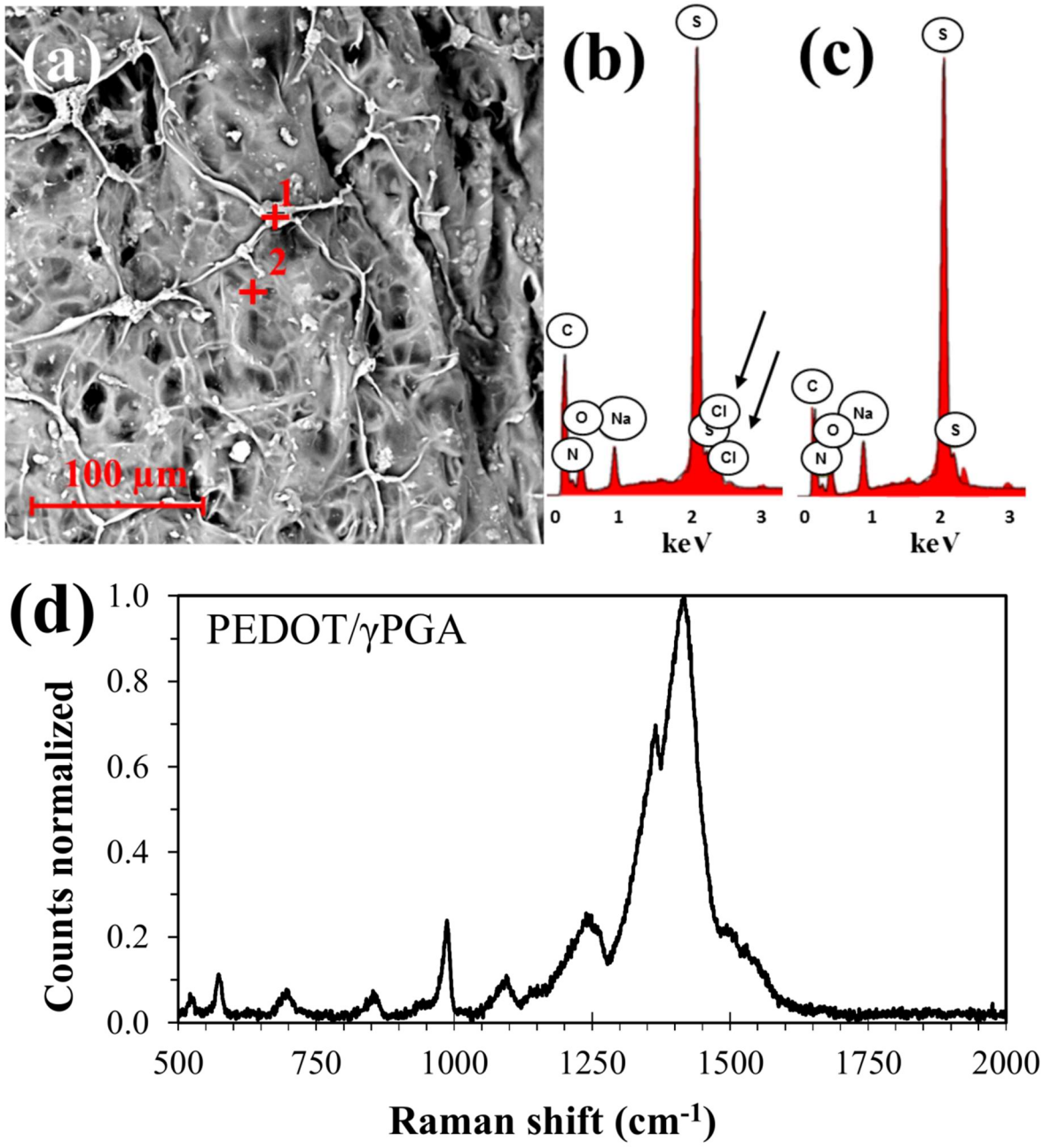

Figure 2. (a) Surface SEM micrograph of the PEDOT/γPGA hydrogel. EDX analyses determined on the (b) point 1 (PEDOT MPs) and on the (c) point 2 (γPGA matrix) of the sample displayed in (a). Cl signal is highlighted with two arrows in (b) to show the main difference with (c). (d) Raman spectra of PEDOT/γ-PGA. Excitation wavelength: 785 nm.

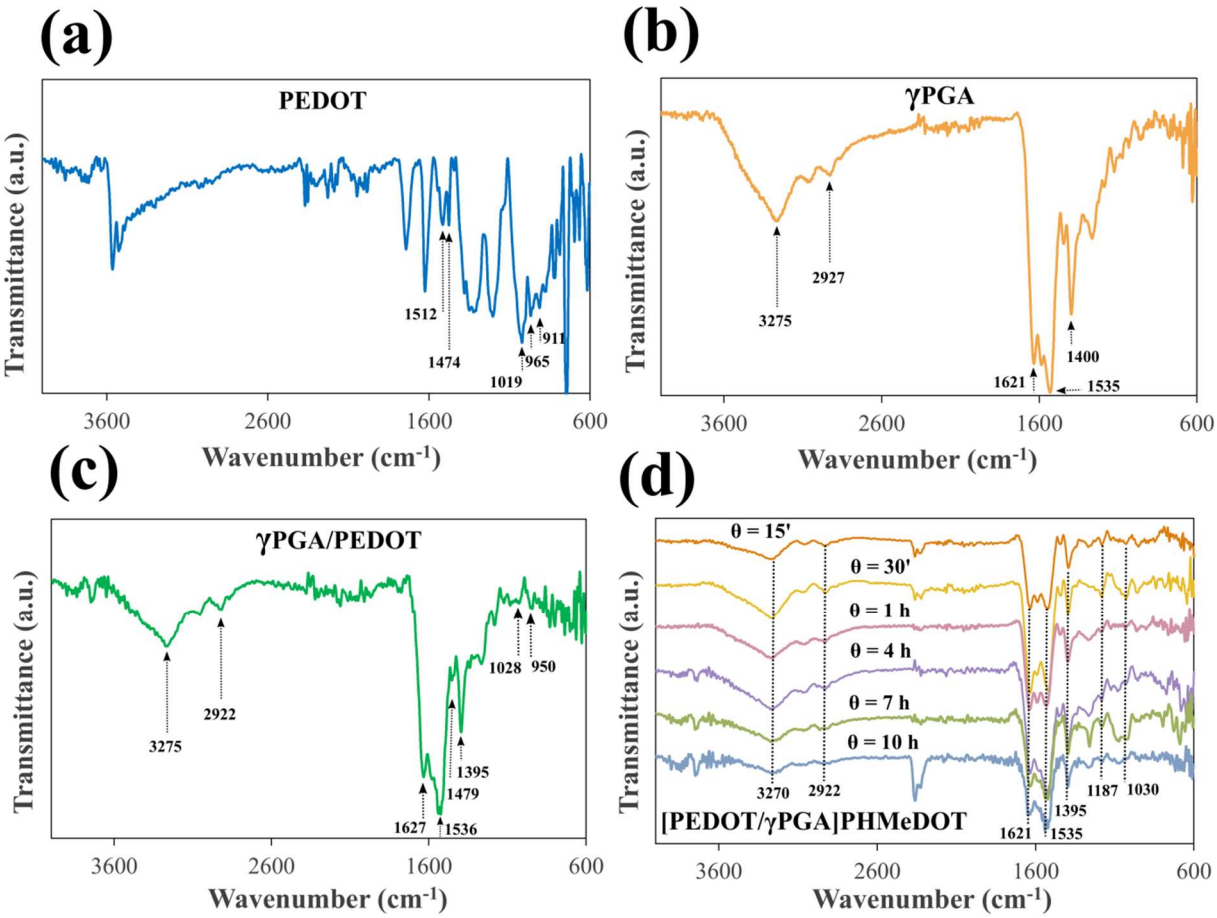

Figure 3. FTIR spectra of (a) PEDOT MPs, (b) γPGA hydrogel, (c) PEDOT/γPGA hydrogel, and (d) [PEDOT/γPGA]PHMeDOT hydrogels obtained using different polymerization times θ.

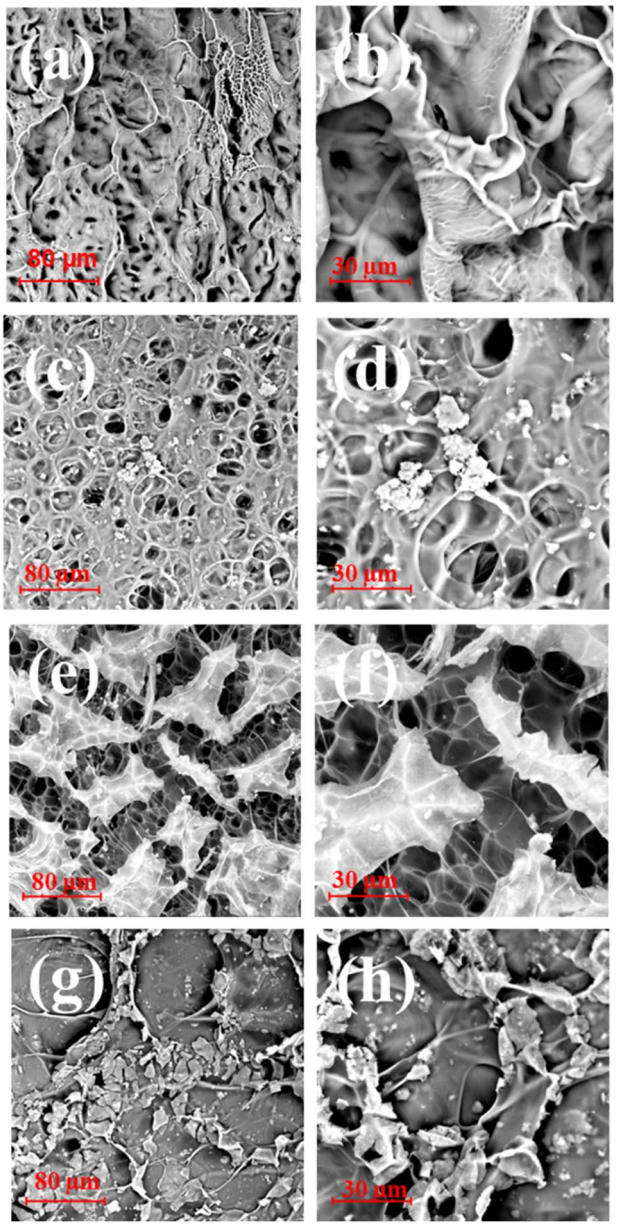

Figure 4. Morphology of freeze-dried hybrid hydrogels. Representative SEM images of (a, b) γPGA hydrogel, (c, d) PEDOT/γPGA, (e, f) [PEDOT/γPGA]PHMeDOT (θ = 1 h), and (g, h) [PEDOT/γPGA]PHMeDOT (θ = 4 h). Micrographs recorded with both (a, c, e, g) 1 kX and (b, d, f, h) 2.3 kX magnifications are displayed.

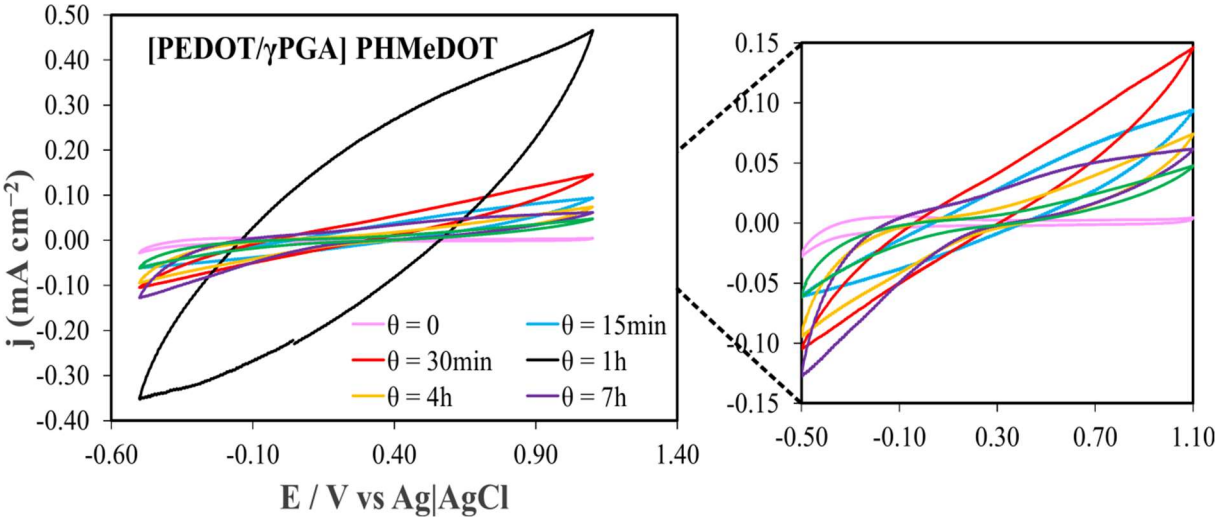

Figure 5. Control voltammograms (2nd cycle) for [PEDOT/γPGA]PHMeDOT prepared using different electropolymerization times (θ = 0, 15 min, 30 min, 1 h, 4 h, 7 h and 10h). Initial and final potential, −0.50; reversal potential, 1.10 V; scan rate of 100 mV s^{-1}.

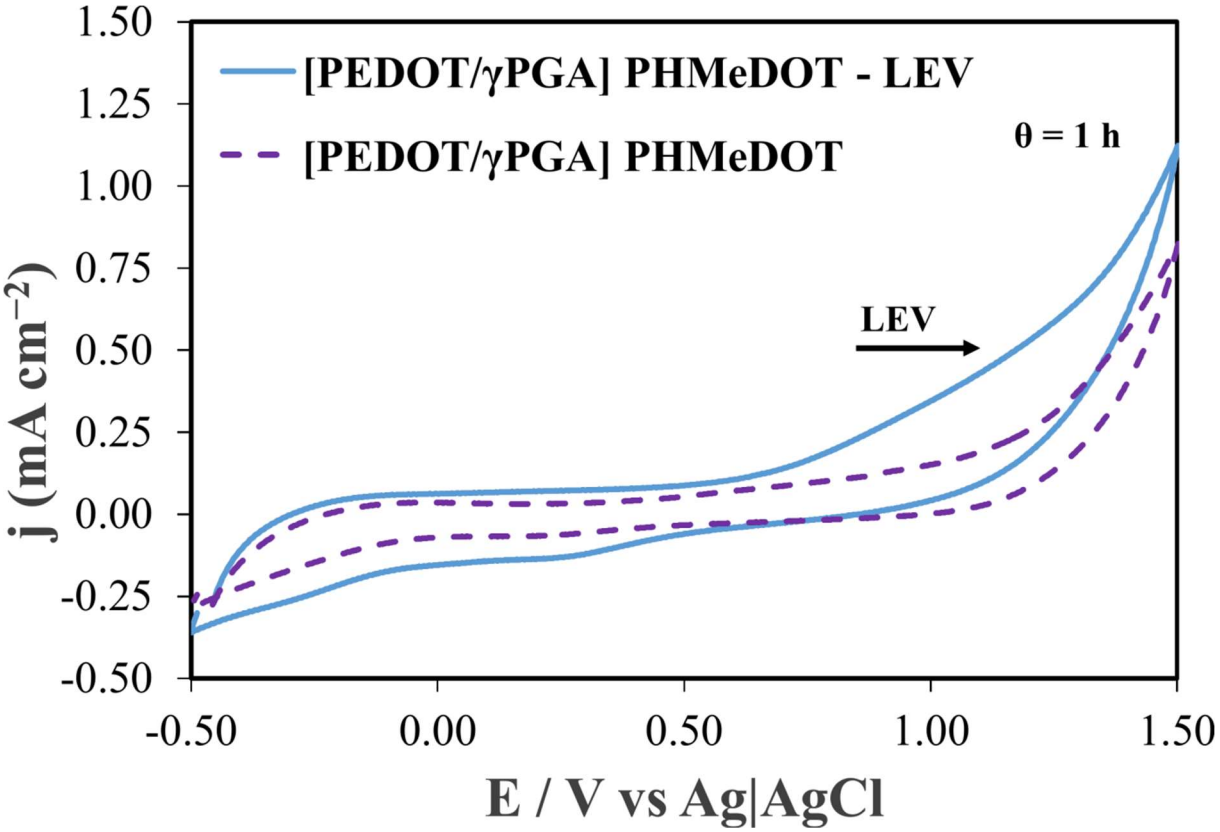

Figure 6. Second voltammogram of [PEDOT/γPGA]PHMeDOT (θ = 1 h) in 0.1M $LiClO_4$ solution; with (blue solid line) and without (purple dashed line) 0.2 mM of LEV. Initial and final potential, −0.50 V; reversal potential, +1.50 V; scan rate of 50 mV s^{-1}.

Table 1. Swelling Ratio (SR, in %) of γPGA, PEDOT/γPGA and [PEDOT/γPGA]PHMeDOT Hydrogels Systems at Different Anodic Polymerization Times (θ).

System	SR (in %)
γPGA	8052 ± 1176
PEDOT/γPGA	6324 ± 910
[PEDOT/γPGA] PHMeDOT (θ = 15 min)	5802 ± 85
[PEDOT/γPGA]PHMeDOT (θ = 30 min)	6319 ± 913
[PEDOT/γPGA/]PMeDOT (θ = 1 h)	6805 ± 1018
[PEDOT/γPGA]PHMeDOT (θ = 4 h)	5435 ± 319
[PEDOT/γPGA]PHMeDOT (θ = 7 h)	4948 ± 1017
[PEDOT/γPGA]PHMeDOT (θ = 10 h)	5257 ± 1736

Table 2. Loss of Electroactivity (LEA at 30th cycle, in %) and Specific Capacitance Values (SC, in mF cm^{-2}) Determined from CV curves at the 2nd and 30th cycles for γPGA, PEDOT/γPGA and [PEDOT/γPGA] PHMeDOT Hydrogels Systems at Different Anodic Polymerization Times (θ).

System	LEA (in %)	SC (in mF cm^{-2})	
	Cycle 30	Cycle 2	Cycle 30
γ-PGA	46	$8 \cdot 10^{-3}$	$5 \cdot 10^{-3}$
PEDOT/γPGA	39	$8 \cdot 10^{-2}$	$6 \cdot 10^{-2}$
[PEDOT/γPGA]PHMeDOT (θ = 15 min)	16	3.1	2.9
[PEDOT/γPGA]PHMeDOT (θ = 30 min)	17	1.2	1.1
[PEDOT/γPGA]PMeEDOT (θ = 1 h)	-9	4.4	4.6
[PEDOT/γPGA]PHMeDOT (θ = 4 h)	23	0.6	0.6
[PEDOT/γPGA]PHMeDOT (θ = 7 h)	5	0.7	0.7
[PEDOT/γPGA]PHMeDOT (θ = 10 h)	20	0.4	0.3

Brenda G. Molina, Ariadna Llampayas, Georgina Fabregat, Francesc Estrany,* Carlos Alemán,* and Juan Torras*

Electroactive Interpenetrated Biohydrogels as Hybrid Materials Based on Conducting Polymers

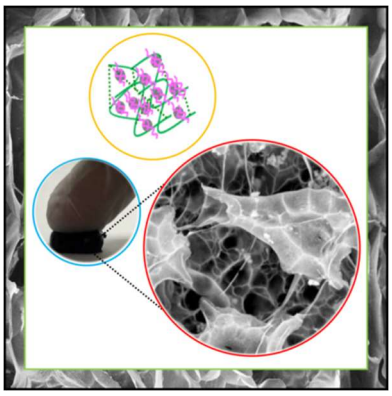

Interpenetration of poly(hydroxymethyl-3,4-ethylenedioxythiophene) (PHMeDOT) inside a poly-γ-glutamic acid (γPGA) biohydrogel matrix, previously loaded with microparticles of poly(3,4-ethylenedioxythiophene) (PEDOT) have been studied and optimized. The morphological and electrochemical properties of the resulting biohydrogel are influenced by the degree of interpenetration.